# Spectral Methods for the Euler Equations: Part II—Chebyshev Methods and Shock Fitting

M. Y. Hussaini,* D. A. Kopriva,† M. D. Salas,‡ and T. A. Zang§
*NASA Langley Research Center, Hampton, Virginia*

**The Chebyshev spectral collocation method for the Euler gasdynamic equations is described. It is used with shock fitting to compute several two-dimensional gasdynamic flows. Examples include a shock/acoustic wave interaction, a shock/vortex interaction, and the classical blunt-body problem. With shock fitting, the spectral method has a clear advantage over second-order finite differences in that equivalent accuracy can be obtained with far fewer grid points.**

## Nomenclature

$a$ = sound speed
$A$ = pressure wave amplitude
$b$ = vortex softening length
$B,C$ = coefficient matrices in Euler equations
$\bar{c}_j$ = constants in discrete Chebyshev transform
$(k_x,k_y)$ = wave vector
$k$ = wave vector magnitude
$L$ = discrete spatial operator
$M,N$ = number of collocation points
$M_s$ = shock Mach number
$p$ = pressure
$P$ = logarithm of pressure
$Q$ = vector of dependent variables in the Euler equations
$Q_{pq}$ = spectral coefficients of $Q$
$Q_{p,q}^{(1,0)}$ = spectral coefficients of $Q_x$
$Q_{pq}^{(0,1)}$ = spectral coefficients of $Q_y$
$(r,\theta)$ = physical polar coordinates
$r_b$ = blunt-body boundary
$r_s$ = shock front radius
$R$ = source term in the Euler equations
$R^+,R^-$ = linearized one-dimensional Riemann variables
$s(t)$ = startup function for linear waves
$S$ = entropy (divided by specific heat at constant volume)
$t$ = physical time
$t_s$ = startup time for linear waves
$T$ = computational time
$u$ = solution to one-dimensional test problems
$\tilde{u}$ = interpolating polynomial
$u_j$ = solution at collocation points
$\hat{u}_n$ = discrete Chebyshev coefficient
$(u,v)$ = physical velocities
$(U,V)$ = contravariant velocity components
$x_j$ = collocation point
$x_L$ = computational left boundary
$x_s$ = shock front location
$(x,y)$ = physical Cartesian coordinates
$(x_0,y_0)$ = center of downstream vortex
$(X,Y)$ = computational coordinates
$y_\ell$ = periodicity length in $y$
$\beta$ = vertical stretching parameter
$\gamma$ = ratio of specific heats
$\Delta x$ = mesh size
$\Delta t$ = time increment
$\theta_c$ = filter cutoff angle
$\theta_I$ = incident angle of pressure wave
$\theta_{\max}$ = angle of computational outflow boundary
$\kappa$ = vortex circulation
$\rho$ = density
$\sigma$ = smoothing function
$\tau_n$ = Chebyshev polynomial of degree $n$
$\psi$ = stream function

Presented as part of Paper 83-1942 at the AIAA Sixth Computational Fluid Dynamics Conference, Danvers, Mass., July 13-15, 1983; received Aug. 5, 1983; revision received Jan. 27, 1984. This paper is declared a work of the U.S. Government and therefore is in the public domain.

*Senior Staff Scientist, Institute of Computer Applications in Science and Engineering. Associate Fellow AIAA.
†Staff Scientist, Institute of Computer Applications in Science and Engineering. Member AIAA.
‡Aerospace Technologist. Associate Fellow AIAA.
§Aerospace Technologist. Member AIAA.

## Introduction

A CONVINCING case has not yet emerged for the spectral shock-capturing technique for the Euler equations. Although solutions can be obtained by such a method, their accuracy tends to be quite low. The filtering procedures necessary to control the oscillations arising from the discontinuity in the solution at the shock have the side effect of reducing the accuracy in the structured regions of the flow. In a previous paper,[1] we reported our experience with a spectral shock-capturing method on a periodic, one-dimensional compressible flow problem. We found the method to be only first-order accurate and certainly no better than finite difference solutions.

In the present paper, we propose a straightforward cure for the oscillations that plague spectral shock-capturing methods: resort to spectral shock-fitting methods instead.

## Spectral Methods for Shock Fitting

Shock-fitting techniques have been a standard finite difference tool for some 15 years.[2,3] They are suitable for problems in which the general features of the solution (but not the details) are predictable. This approach overcomes the difficulties of shock-induced oscillations for the simple reason that the shock front itself is a computational boundary. While it eliminates the need for computing derivatives across the shock (which is the source of the oscillations), it adds the complexity of requiring an algorithm to determine the shape and motion of the shock. Spectral methods for shock fitting are a straightforward combination of both standard techniques. They do, however, require the use of Chebyshev polynomials rather than Fourier series in at least one coordinate direction. We begin this section by discussing the fundamentals of the Chebyshev spectral methods.

### Basic Chebyshev Spectral Concepts

Consider the model problem

$$u_t + u_x = 0 \tag{1}$$

on $-1 \le x \le 1$ with initial condition

$$u(x,0) = \sin(2.5\pi x) \tag{2}$$

and boundary condition

$$u(-1,t) = \sin[2.5\pi(-1-t)] \tag{3}$$

The expansion functions are the Chebyshev polynomials

$$\tau_n(x) = \cos(n\cos^{-1}x) \tag{4}$$

and the collocation points are

$$x_j = \cos(\pi j/N) \qquad j = 0,1,\ldots,N \tag{5}$$

Note that

$$\tau_n(x_j) = \cos(\pi jn/N) \tag{6}$$

The discrete Chebyshev coefficients are

$$\hat{u}_n = \frac{2}{N\bar{c}_n}\sum_{j=0}^{N}\bar{c}_j^{-1}u_j\cos\frac{\pi jn}{N} \tag{7}$$

where

$$\begin{aligned}\bar{c}_n &= 2 \qquad n = 0 \text{ or } N\\ &= 1 \qquad 1 \le n \le N-1\end{aligned} \tag{8}$$

Thus the interpolating function is

$$\tilde{u}(x) = \sum_{n=0}^{N}\hat{u}_n\tau_n(x) \tag{9}$$

The analytic derivative of this function is

$$\frac{\partial\tilde{u}}{\partial x} = \sum_{n=0}^{N}\hat{u}_n^{(1)}\tau_n(x) \tag{10}$$

where

$$\hat{u}_{N+1}^{(1)} = 0, \qquad \hat{u}_N^{(1)} = 0$$

$$\bar{c}_n\hat{u}_n^{(1)} = \hat{u}_{n+2}^{(1)} + 2(n+1)\hat{u}_{n+1}, \quad n = N-1, N-2,\ldots,0 \tag{11}$$

The Chebyshev spectral derivatives at the collocation points are

$$\left.\frac{\partial\tilde{u}}{\partial x}\right|_j = \sum_{n=0}^{N}\hat{u}_n^{(1)}\cos\frac{\pi jn}{N} \tag{12}$$

Special versions of the fast Fourier transform (FFT) may be used for evaluating the sums in Eqs. (7) and (12). The total cost for a Chebyshev spectral derivative is thus $\mathcal{O}(N\ell nN)$.

The time-stepping scheme for Eq. (1) must use the boundary condition to update $u_N$ (at $x=-1$) and the approximate derivatives from Eq. (12) to update $u_j$ for $j=0,1,\ldots,N-1$. Note that no special formula is required for the derivative at $j=0$ (or $x=+1$). Results at $t=1$ for a Chebyshev spectral method, a Fourier spectral method, and a second-order finite difference method are given in Table 1. (The temporal discretization errors are negligible in all cases.) For this nonperiodic problem, the Fourier spectral methods are quite inappropriate, but the Chebyshev spectral method is far superior to the finite difference method.

The Chebyshev collocation points are the extreme points of $\tau_N(x)$. Note that they are not evenly distributed in $x$, but rather are clustered near the endpoints. The smallest mesh size scales as $1/N^2$. While this distribution contributes to the quality of the Chebyshev approximation and permits the use of the FFT in evaluating the series, it also places a severe time-step limitation on explicit methods for evolution equations.

### Filtering for Chebyshev Spectral Methods

The same types of filtering operations that were discussed in Ref. 1 for Fourier spectral methods are applicable to Chebyshev spectral methods as well. However, in the latter case, there is as yet no theoretical support for the usefulness of preprocessing or derivative filtering on simple linear problems.

A straightforward filtering procedure is to mimic Eq. (8) of Ref. 1 by setting

$$u_j = \sum_{n=0}^{N}\sigma\left(\frac{n\pi}{N}\right)\hat{u}_n\cos\left(\frac{n\pi j}{N}\right) \tag{13}$$

where $\hat{u}_n$ is given by Eq. (7) and $\sigma(\theta)$ is a standard smoothing function as described in Ref. 1. There are two problems with this approach: boundary conditions and conservation properties. Neither survives under this type of filtering. The lack of conservation in filtering does not appear to be crucial. After all, the shocks are not being captured and, as will be evident below, the computations use the Euler equations in nonconservation form. Any drift in the mean flow properties in the calculations has been minor. The boundary conditions are another matter. They are enforced after every application of filtering.

### A Spectral Shock-Fitted Method

A schematic of the type of spectral shock-fitted calculations described below is illustrated in Fig. 1. At time $t=0$ an infinite, normal shock at $x=0$ separates a rapidly moving, uniform fluid on the left from the fluid on the right, which is in a quiescent state except for some specified fluctuation. The initial conditions are chosen so that, in the absence of any fluctuation, the shock moves uniformly in the positive $x$ direction with a Mach number (relative to the fluid on the right) denoted by $M_s$. In the presence of fluctuations, the shock front will develop ripples. The shape of the shock is described by the function $x_s(y,t)$. The numerical calculations

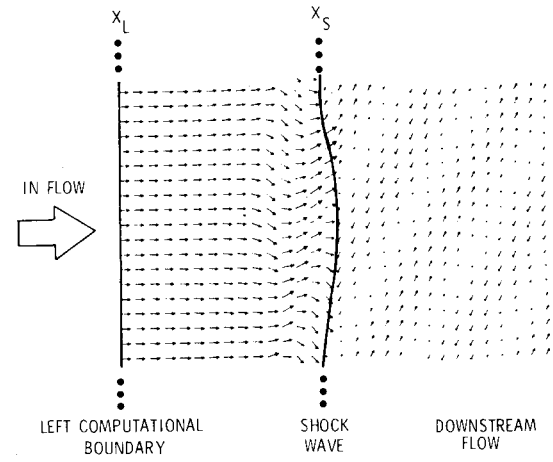


**Fig. 1 Typical shock-fitted time-dependent flow model in the physical plane.**

**Table 1 Maximum error for a one-dimensional Dirichlet problem**

| $N$ | Chebyshev spectral | Fourier spectral | Finite difference |
|---|---|---|---|
| 4 | 1.49 (0) | 1.85 (0) | 1.64 (0) |
| 8 | 6.92 (−1) | 1.92 (0) | 1.73 (0) |
| 16 | 1.50 (−4) | 2.27 (0) | 1.23 (0) |
| 32 | 3.45 (−11) | 2.28 (0) | 3.34 (−1) |
| 64 | 9.55 (−11) | 2.27 (0) | 8.44 (−2) |

are used to determine the state of the fluid in the region between the shock front and some suitable left boundary $x_L(t)$ and also to determine the motion and shape of the shock front itself.

Figure 1 is taken from a shock/turbulence calculation[4] in which the downstream fluctuation is a plane vorticity wave that is periodic in $y$ with period $y_\ell$. Because of the initial value nature of the calculation, the fluid motion behind the shock is not periodic in $x$, as Fig. 1 makes abundantly clear. The interesting physical domain is given by

$$x_L(t) \le x \le x_s(y,t) \tag{14a}$$

$$0 \le y \le y_\ell \tag{14b}$$

$$t \ge 0 \tag{14c}$$

The change of variables

$$X = \frac{x - x_L(t)}{x_s(y,t) - x_L(t)} \tag{15a}$$

$$Y = y/y_\ell \tag{15b}$$

$$T = t \tag{15c}$$

produces the computational domain

$$0 \le X \le 1, \quad 0 \le Y \le 1, \quad T \ge 0 \tag{16}$$

The fluid motion is modeled by the two-dimensional Euler equations. In terms of the computational coordinates, these are

$$Q_T + BQ_X + CQ_Y = 0 \tag{17}$$

where $Q = (P,u,v,S)^T$,

$$B = \begin{pmatrix} U & \gamma X_x & \gamma X_y & 0 \\ \frac{a^2}{\gamma} X_x & U & 0 & 0 \\ \frac{a^2}{\gamma} X_y & 0 & U & 0 \\ 0 & 0 & 0 & U \end{pmatrix} \tag{18}$$

and

$$C = \begin{pmatrix} V & \gamma Y_x & \gamma Y_y & 0 \\ \frac{a^2}{\gamma} Y_x & V & 0 & 0 \\ \frac{a^2}{\gamma} Y_y & 0 & V & 0 \\ 0 & 0 & 0 & V \end{pmatrix} \tag{19}$$

The contravariant velocity components are given by

$$U = X_t + uX_x + vX_y \quad \text{and} \quad V = Y_t + uY_x + vY_y \tag{20}$$

where a subscript denotes partial differentiation with respect to the indicated variable. Reference conditions at downstream infinity are used to normalize $p$ and $S$; $u$ and $v$ are velocity components in the $x$ and $y$ directions, both scaled by the characteristic velocity defined as the square root of the pressure/density ratio at downstream infinity. A value $\gamma = 1.4$ has been used.

Let $n$ denote the time level and $\Delta t$ the time increment. The time discretization of Eq. (17) is

$$\tilde{Q} = [I - \Delta t L^n] Q^n \tag{21}$$

$$Q^{n+1} = \tfrac{1}{2}[Q^n + (I - \Delta t \tilde{L})\tilde{Q}] \tag{22}$$

where $L$ denotes the spatial discretization of $B\partial_X + C\partial_Y$. The solution $Q$ has the Chebyshev-Fourier series expansion

$$Q(X,Y,T) = \sum_{p=0}^{M} \sum_{q=-N/2}^{N/2-1} Q_{pq}(T)\tau_p(\xi)e^{2\pi i q Y} \tag{23}$$

where $\xi = 2X - 1$. The derivatives $Q_X$ and $Q_Y$ are approximated by

$$Q_X = 2\sum_{p=0}^{M} \sum_{q=-N/2}^{N/2-1} Q_{pq}^{(1,0)}(T)\tau_p(\xi)e^{2\pi i q Y} \tag{24}$$

$$Q_Y = 2\pi\sum_{p=0}^{M} \sum_{q=-N/2}^{N/2-1} Q_{pq}^{(0,1)}(T)\tau_p(\xi)e^{2\pi i q Y} \tag{25}$$

where $Q_{pq}^{(1,0)}$ is computed from $Q_{pq}$ in a manner analogous to Eq. (11) and

$$Q_{pq}^{(0,1)} = iqQ_{pq} \tag{26}$$

The most critical part of the calculation is the treatment of the shock front. The shock-fitting approach used here is desirable because it avoids the severe postshock oscillations that plague shock-capturing methods. The time derivative of the Rankine-Hugoniot relations provides an equation for the shock acceleration. This equation is integrated to update the shock position (see Ref. 5 for details). This method is a generalization of the finite difference method developed by Pao and Salas[6] for their study of the shock/vortex interaction.

#### Boundary Conditions

The correct boundary conditions on the left depend upon the relative Mach number. For uniform flow and $\gamma = 1.4$, the flow behind the shock is supersonic if $M_s \ge 2.08$. In this case, at $X_L$ there is a supersonic inflow boundary at which it is appropriate to specify all variables. If $M_s < 2.08$, there is a subsonic inflow boundary on the left. Then, the advisable procedure is to base the numerical boundary conditions on the linearized characteristics of the Euler equations. At the left (subsonic) boundary, the (linearized) characteristic variables corresponding to the outgoing characteristic direction are

$$R^- = P - (\gamma/a)u \tag{27}$$

Similarly,

$$R^+ = P + (\gamma/a)u \tag{28}$$

corresponds to the outgoing characteristic direction at the right (subsonic) boundary used by the shock-fitting algorithm.

A set of successful boundary conditions on the left is obtained by first calculating the preliminary values of all quantities at the left boundary and then incorporating the

given values of $S$, $v$, and $R^+$ as

$$S=S_{\text{given}}, \quad v=v_{\text{given}}$$

$$P+(\gamma/a)u=R^+_{\text{given}}, \quad P-(\gamma/a)u=P_{\text{prelim}}-(\gamma/a)u_{\text{prelim}} \quad (29)$$

Thus, the partial differential equation is used to update the appropriate characteristic combination of the variables at the boundary. The characteristic analysis is given in Ref. 7. The particular boundary condition was advocated in Ref. 8. For the right boundary, a similar characteristic correction procedure can be incorporated into the evaluation of the shock velocity.

The global nature of spectral methods makes them even more sensitive to the boundary conditions than finite difference methods. An illustration of just how unforgiving spectral methods can be is provided in Fig. 2. Shown there are two spectral shock-fitted calculations of the interaction of a Mach 1.3 shock with a von Kármán vortex street. (See Ref. 9 for more details about this problem.) The top row shows what happens when all flow variables are specified at the left, subsonic, inflow boundary, whereas the bottom row displays a calculation that is identical except for the use of Eq. (29) as the inflow boundary condition. The former calculation is clearly contaminated by oscillations emanating from the inflow boundary. The latter calculation makes clear that no physical signals have yet reached the inflow location, even though in the spectral method numerical signals reach the inflow instantaneously. Finite difference calculations for this same problem were reported in Ref. 9. Despite the fact that an overspecified inflow boundary condition was used, no analogous problem arose because of the local nature of the discretization.

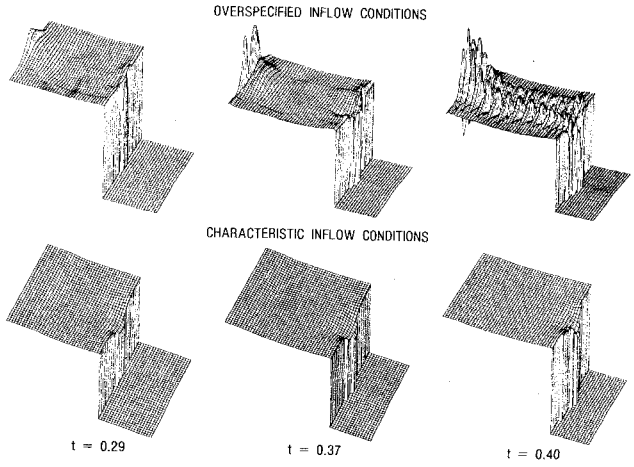


**Fig. 2 Spectral pressure distribution for a Mach 1.3 Karman vortex street showing sensitivity to inflow boundary conditions.**

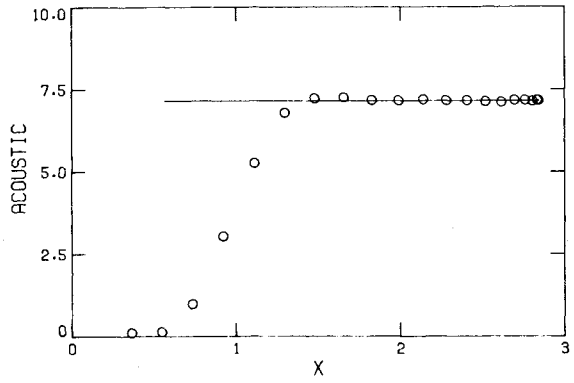


**Fig. 3 Post-shock dependence of the pressure response to a pressure wave incident at 10 deg to a Mach 3 shock (solid line is the linear theory prediction, circles the spectral solution).**

## Results for Chebyshev Spectral Shock Fitting

### Shock/Turbulence Interaction

The nonlinear interaction of plane waves with shocks was examined at length in Ref. 4. The numerical method used there was similar to the one described above, but employed second-order finite differences in place of the present Chebyshev-Fourier spectral discretization. Detailed comparisons were made in Ref. 4 with the predictions of linear theory.[10] The linear results turned out to be surprisingly robust, remaining valid at very low (but still supersonic) Mach numbers and at very high incident wave amplitudes. The only substantial disagreement occurred for incident waves whose fronts were nearly perpendicular to the shock front. This type of shock/turbulence interaction is a useful test of the spectral technique because the method can be calibrated in the regions for which linear theory has been shown to be valid.

The most reliable numerical results can be obtained for the acoustic responses to acoustic waves. Unlike the vorticity responses, these require no differentiation of the flow variables, thus eliminating one extra source of error. Moreover, the acoustic response stretches much further behind the shock than the vorticity response, thus providing greater statistical reliability. Vorticity response results are reported in Ref. 11. The incident pressure wave is taken to be

$$p_I'=A_I' e^{i(k_I\cdot x-\omega_I t)} \quad (30)$$

where $k_I=(k_{I,x}k_{I,y})$, $\omega_I=M_s a_I k_{I,x}+a_I k_I$, and $A_I'$ is the amplitude. In terms of the incidence angle $\theta_I$, $k_I=(k_I\cos\theta_I, k_I\sin\theta_I)$. The linearized transmitted acoustic wave can be expressed in the same manner with all subscripts changed from 1 to 2. The amplification coefficient for the transmitted acoustic wave is then the ratio $A_2'/A_1'$. Figure 3 indicates the transmission coefficient extracted from the computation. At each fixed value of $X$, we perform a Fourier analysis in $Y$ of the pressure. The Fourier coefficient for $q=1$ provides the amplitude $A_2'$. In order to reduce the transients that would accompany an abrupt start of the calculation at full wave amplitude, an extra factor of $s(t)$ is inserted into Eq. (30), where

$$s(t)=3(t/t_s)^2-2(t/t_s)^3 \qquad 0\le t\le t_s$$
$$=1 \qquad t\ge t_s \quad (31)$$

The startup time $t_s$ is some multiple (typically ½) of the time it takes the shock to encounter one full wavelength (in the $x$ direction) of the incident wave. The ratio $A_2'/A_1'$ is plotted in Fig. 3 as a function of the mean value of the physical coordinate $x$ corresponding to $X$. The startup time for this Mach 3 case is $t_s=0.56$. The average of the $x$-dependent responses between the startup interval and the shock produces the computed transmission coefficient. The standard deviation of the individual responses serves as an error estimate.

The dependence upon incidence angle of the acoustic transmission coefficient for $A_I'=0.001$ and $M_s=3$ waves is displayed in Fig. 4. As is discussed in Ref. 4, linear theory is quite reliable at angles below, say, 45 deg. Figure 4 contains results from both spectral and finite difference calculations. The finite difference results were obtained with the same second-order MacCormack's method that was described in Ref. 4, except that periodic boundary conditions (rather than stretching) were employed in the $y$ direction. The finite difference grid was $64\times16$ and these calculations used a CFL number of 0.70. The spectral grid was $32\times8$ with a CFL number of 0.50. (No solution smoothing was applied.) Figure 4 shows that both methods produce the same results. A head-to-head comparison of both methods for the $\theta_I=10$ deg case

**Table 2 Grid dependence of acoustic transmission coefficient**

| Grid | Finite difference | Chebyshev-Fourier spectral |
|---|---|---|
| 16×4 | 6.403 ± 2.652 | 7.257 ± 0.587 |
| 16×8 | 6.427 ± 2.626 | 7.257 ± 0.587 |
| 32×4 | 7.105 ± 0.453 | 7.158 ± 0.022 |
| 32×8 | 7.134 ± 0.471 | 7.158 ± 0.022 |
| 32×16 | 7.139 ± 0.497 | 7.158 ± 0.022 |
| 64×16 | 7.163 ± 0.078 | 7.157 ± 0.017 |
| 128×16 | 7.152 ± 0.022 | |
| "Exact" | 7.156 | 7.156 |

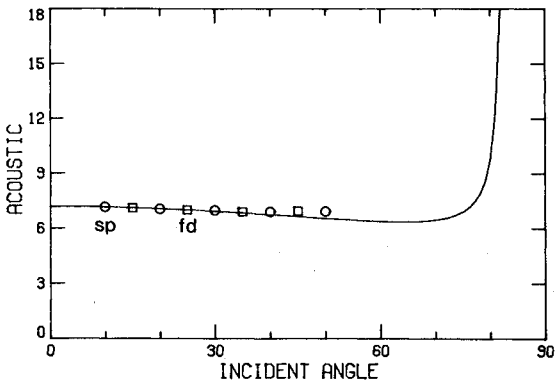


**Fig. 4 Dependence on incident angle of the pressure response to a 0.1% amplitude pressure wave incident on a Mach 3 shock (solid line is the linear theory result, circles spectral solutions, and squares finite difference solutions).**

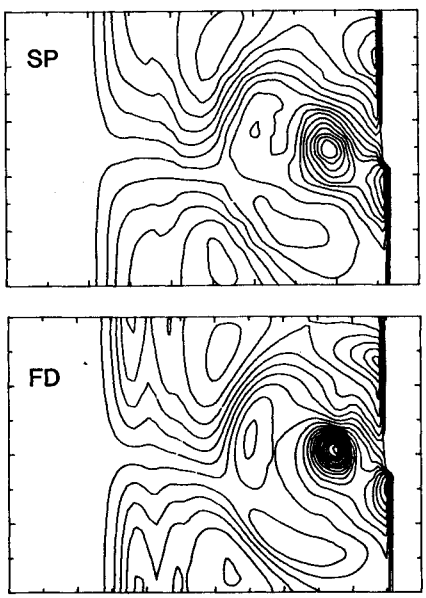


**Fig. 5 Pressure contours for spectral (SP) and finite difference (FD) calculations of the shock/vortex interaction problem. The spectral solution used a 32×16 grid and the finite difference used a 75×50 grid.**

is provided in Table 2. The "exact" value is taken from linear theory.[10] Since the amplitude of the incident acoustic wave is so small, it should come as no surprise that four points in the $y$ direction suffice for the spectral calculation. Note that the standard deviations are substantially smaller for the spectral method. These results suggest that the spectral method requires only half as many grid points in each coordinate direction.

**Table 3 Comparison of stagnation pressures for uniform flow past a circular cylinder**

| Mach No. | Calculated pressure | Theoretical pressure | Relative error, % |
|---|---|---|---|
| 2 | 5.651 | 5.6408 | 0.18 |
| 4 | 21.072 | 21.0750 | −0.014 |
| 6 | 46.846 | 46.8109 | 0.075 |

### Shock/Vortex Interaction

This problem is closely related to the previous one. The downstream field is not the linear plane pressure wave of Eq. (30), but an idealized vortex in which the density is constant and the velocities are derivable from the stream function

$$\psi = (\kappa/2\pi)\log\sqrt{b^2 + (x-x_0)^2 + (y-y_0)^2} \tag{32}$$

the pressure from Bernoulli's equation, and the temperature from the equation of state. This model approaches an idealized incompressible point vortex at large distances from the vortex center at $(x_0,y_0)$, but it is much smoother in the core. The specific example provided here has the circulation $\kappa=0.40$, the vortex softening scale $b=0.1$, and the vortex located at $(x_0,y_0)=(0.5,0.0)$.

Note that periodic boundary conditions in $y$ are no longer appropriate. Accordingly, Eqs. (14b) and (15b) are replaced by

$$-\infty < y < \infty \tag{33a}$$

and

$$Y = [\tanh(\beta y) + 1]/2 \tag{33b}$$

respectively, where the stretching parameter $\beta$ is of order one. Moreover, the spectral method now uses Chebyshev series in $Y$ as well as $X$. The analogs of Eqs. (14-26) are given in full in Ref. 9. (Incidentally, it was this Chebyshev-Chebyshev algorithm that was used in the production of Fig. 2.)

The computed results for the shock/vortex interaction at $t=0.35$ are given in Fig. 5 for both finite difference and spectral methods. The contour levels are the same in the two diagrams. The finite difference calculation used a 75×50 grid, whereas the spectral result was obtained with a 32×16 grid, with a CFL number of 0.50 and solution smoothing using the exponential cutoff applied every 80 time steps. The major difference between the results is that the spectral calculation does not have as deep a pressure minimum as the finite difference result.

### Supersonic Flow Past a Circular Cylinder

The classical problem of a blunt body, such as a circular cylinder in a supersonic stream, has been an ideal test problem for numerical methods because it provides a relatively simple well-posed transonic problem with nontrivial initial and boundary conditions. The present spectral method obtains the steady-state solution as the time asymptotic solution of the unsteady Euler equations written in the cylindrical polar coordinate $(r,\theta)$ system. The physical domain of interest consists of the known body $r=r_b(\theta)$, the unknown shock location $r=r_s(\theta,t)$, the axis of symmetry (at the front stagnation streamline $\theta=\pi$), and the outflow boundary $\theta=\pi-\theta_{\max}$. For the purpose of shock fitting, the coordinate transformation

$$X = \frac{r-r_b(\theta)}{r_s(\theta,t)-r_b(\theta)} \tag{34a}$$

$$Y = (\pi-\theta)/\theta_{\max} \tag{34b}$$

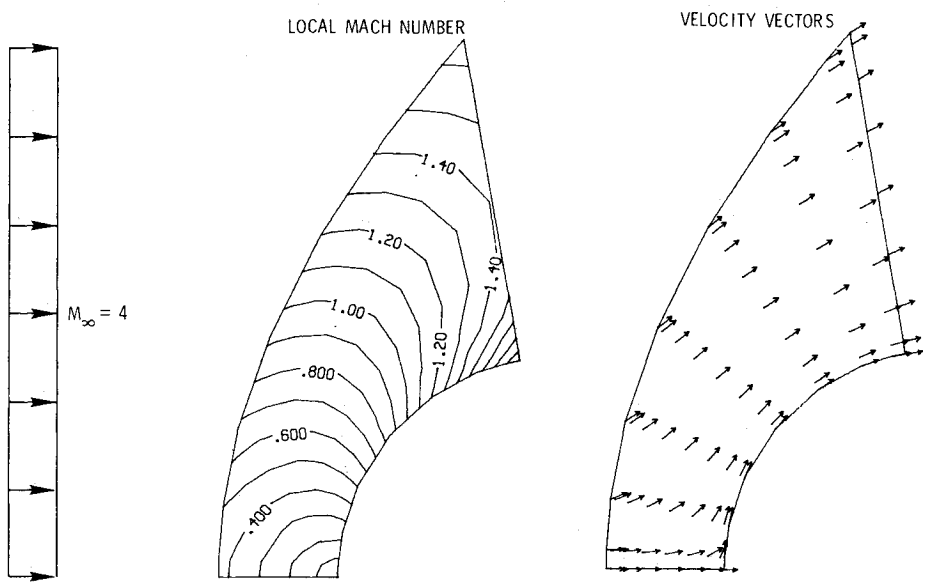


**Fig. 6 Spectral solution on a 9×9 grid for a circular cylinder in a Mach 4 uniform stream.**

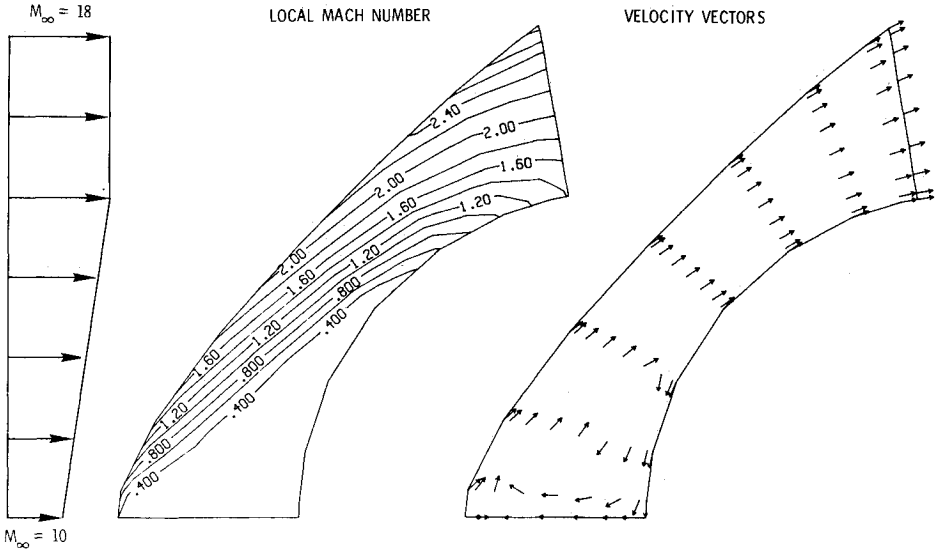


**Fig. 7 Spectral solution on a 9×9 grid for a circular cylinder in a linearly sheared stream.**

is introduced so that the shock wave and body are coordinate lines in the transformed domain. The transformed equations of motion, in the notation of the shock interaction problems, are

$$Q_T + BQ_X + CQ_Y + R = 0 \tag{35}$$

where

$$B = \begin{bmatrix} U & \gamma X_r & (\gamma/r)X_\theta & 0 \\ (a^2/\gamma)X_r & U & 0 & 0 \\ (a^2/\gamma)(1/r)X_\theta & 0 & U & 0 \\ 0 & 0 & 0 & U \end{bmatrix} \tag{36}$$

$$C = \begin{bmatrix} V & \gamma Y_r & (\gamma/r)Y_\theta & 0 \\ (a^2/\gamma)Y_r & V & 0 & 0 \\ (a^2/\gamma)(1/r)Y_\theta & 0 & V & 0 \\ 0 & 0 & 0 & V \end{bmatrix} \tag{37}$$

and

$$R = \left[\gamma\frac{u}{r}, -\frac{v^2}{r}, \frac{uv}{r}, 0\right]^T \tag{38}$$

with

$$U = X_t + uX_r + \frac{v}{r}X_\theta \quad \text{and} \quad V = (v/r)Y_\theta \tag{39}$$

The flowfield variables are expanded in double Chebyshev series and the solution technique is the same as for the previous problem.

The shock boundary $r = r_s(\theta,t)$ (i.e., $X=1$) is computed using the Rankine-Hugoniot jump conditions and the compatibility equation along the outgoing characteristic from the high-pressure side of the shock. On the body $r = r_b(\theta)$ (i.e., $X=0$), the normal component of velocity $u$ is zero. The limiting angle $\theta_{\max}$ is chosen so that the outflow boundary $Y=1$ is supersonic and hence no boundary conditions need be imposed.

At the symmetry line, $\theta=\pi$ (or $Y=0$), the tangential velocity component $v$ is set to zero. The variables $P$, $S$, and $u$ (as well as the shock velocity) satisfy the condition that their derivatives with respect to $Y$ are zero there. This is enforced at

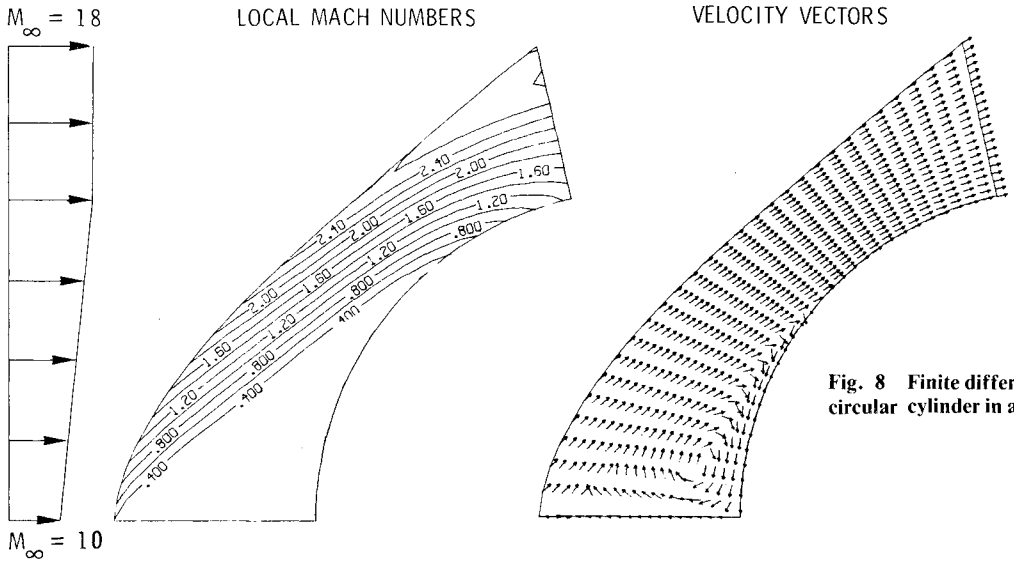


**Fig. 8 Finite difference solution on a $20 \times 30$ grid for a circular cylinder in a linearly sheared stream.**

each stage of the predictor-corrector time discretization [see Eqs. (21) and (22)] by simply using the value zero and not the standard Chebyshev spectral $Y$-derivative values for $P$, $S$, and $u$ at $Y=0$.

The filtering employed in the calculations reported below was solution smoothing every 50 time steps using the quartic taper [Eq. (12) of Ref. 1] with $\theta_c = 2\pi/3$. After each filtering step, the boundary conditions were applied: $u$ was set to zero on the body and $v$ to zero on the symmetry line; moreover, the Neumann boundary conditions at $Y=0$ were enforced by transforming to wave number space, adjusting the very highest Chebyshev coefficient as needed, and then transforming back to physical space.

Several calculations have been performed for the flow of an initially uniform stream past a circular cylinder. The limiting angle $\theta_{\max}$ was 80 deg, the collocation grid $9 \times 9$, and the CFL number 0.20, with 2000 time steps taken. Results for the Mach 4 case are illustrated in Fig. 6. Note that the essential features of the flow are evident even on this very coarse grid. (Indeed, it is the small number of data points that is responsible for the jagged appearance of the contour lines.) Similar results have been obtained for the Mach 2 and 6 situations. Table 3 presents a comparison of the computed values of the stagnation pressure with the theoretical results.[12] Since the numerical computations have converged to only three or four digits after 2000 time steps, the performance of the spectral discretization may be even better than that implied by Table 3. We re-emphasize the fact that there remains the clear need for effective means of surmounting the severe explicit time-step restriction besetting the current Chebyshev spectral methods.

Results for a more challenging flow are shown in Fig. 7. Finite difference results (on a $20 \times 30$ grid) are given in Fig. 8 for comparison. The linearly sheared stream produces a recirculating region. The $9 \times 9$ spectral grid is still capable of resolving this essential feature.

## Conclusions

Our results demonstrate that spectral shock-fitting methods for compressible flows are viable techniques. The quantitative comparison for the shock/acoustic wave problem shows the superior performance of the spectral method. Similar performance is observed on the shock/vortex and blunt-body problems when the spectral results are compared with finite difference results obtained on a much finer grid.

Our experience shows that, before the full potential of spectral methods is realized, several aspects must be improved. First, filtering techniques for both Fourier and Chebyshev methods need to be refined. For filtering in Chebyshev methods, the problem of conservation and boundary conditions must be resolved. Finally, for nonperiodic problems, the collocation grid distribution imposes a severe restriction on the explicit time stepping used throughout this paper. On the other hand, implicit time stepping involves expensive inversion of full matrices. There is a clear need to develop efficient acceleration techniques.

## Acknowledgments

Research by the first and second authors was supported by the National Aeronautics and Space Administration under NASA Contracts NAS1-17070 and NAS1-17130 while they were in residence at ICASE, NASA Langley Research Center, Hampton, Va.

## References

[1] Hussaini, M. Y., Kopriva, D. A., Salas, M. D., and Zang, T. A., "Spectral Methods for the Euler Equations: Part I—Fourier Methods and Shock-Capturing," *AIAA Journal*, Vol. 23, Jan. 1985, pp. 64-70.

[2] Moretti, G., "Inviscid Blunt Body Shock Layers," Polytechnic Institute of Brooklyn, New York, PIBAL Rept. 68-15, June 1968.

[3] Moretti, G., "Thoughts and Afterthoughts About Shock Computations," Polytechnic Institute of Brooklyn, New York, PIBAL Rept. 72-37, Dec. 1972.

[4] Zang, T. A., Hussaini, M. Y., and Bushnell, D. M., "Numerical Computations of Turbulence Amplification in Shock Wave Interactions," *AIAA Journal*, Vol. 22, Jan. 1984, pp. 13-21.

[5] Hussaini, M. Y., Salas, M. D., and Zang, T. A., "Spectral Methods for Inviscid, Compressible Flows," *Advances in Computational Transonics*, edited by W. G. Habashi, Pineridge Press, Swansea, Wales, March 1984.

[6] Pao, S. P. and Salas, M. D., "A Numerical Study of Two-Dimensional Shock Vortex Interaction," AIAA Paper 81-1205, 1981.

[7] Oliger, J. and Sundström, A., "Theoretical and Practical Aspects of Some Initial Boundary Value Problems in Fluid Dynamics," *SIAM Journal of Applied Mathematics*, Vol. 35, Nov. 1978, pp. 419-446.

[8] Gottlieb, D., Gunzburger, M., and Turkel, E., "On Numerical Boundary Treatment of Hyperbolic Systems for Finite Difference and Finite Element Methods," *SIAM Journal on Numerical Analysis*, Vol. 19, Aug. 1982, pp. 671-682.

[9] Salas, M. D., Zang, T. A., and Hussaini, M. Y., "Shock-Fitted Euler Solutions to Shock-Vortex Interactions," *Proceedings of the 8th International Conference on Numerical Methods in Fluid Dynamics*, edited by E. Krause, Springer-Verlag, New York, 1982, pp. 461-467.

[10] Ribner, H. S., "Shock-Turbulence Interaction and the Generation of Noise," NACA Rept. 1233, 1955.

[11] Zang, T. A., Kopriva, D. A., and Hussaini, M. Y., "Pseudospectral Calculation of Shock Turbulence Interactions," *Proceedings of the 3rd International Conference on Numerical Methods in Laminar and Turbulent Flow*, edited by C. Taylor, Pineridge Press, Swansea, Wales, 1983, pp. 210-220.

[12] Ames Research Staff, "Equations, Tables, and Charts for Compressible Flow," NACA Rept. 1135, 1953.